

Characterization and photocatalytic properties of lutetium ion-doped titanium dioxide photocatalyst

Nahomi Sakaguchi Miyamoto^{1,4} · Ryo Miyamoto² · Elio Giamello³ · Tsutomu Kurisaki¹ · Hisanobu Wakita¹

Received: 2 March 2018 / Accepted: 2 May 2018 / Published online: 21 May 2018
© Springer Science+Business Media B.V., part of Springer Nature 2018

Abstract Lutetium-doped titanium dioxide (Lu-TiO₂) was synthesized using a sol–gel method. The obtained compounds were characterized by X-ray diffraction and electron paramagnetic resonance. The photocatalytic decomposition of adenosine 5′-triphosphate (ATP) under UV irradiation was investigated to estimate the effect of the doped lutetium. Our results showed that the Lu-TiO₂ nanoparticles have higher photoactivity than an undoped TiO₂. Furthermore, the role of lutetium in Lu-TiO₂, the structure of the photoreaction site on Lu-TiO₂ and the reaction mechanism are also discussed.

Keywords Lutetium-doped titanium dioxide · Sol–gel · Photocatalytic decomposition · Electron paramagnetic resonance

Introduction

Photocatalytic properties of titanium dioxide semiconductors (TiO₂) are well established [1–30]. Titanium dioxide is capable of completely oxidizing various hazardous materials to nontoxic products. It has become the benchmark

✉ Ryo Miyamoto
rmiya@hirosaki-u.ac.jp

Tsutomu Kurisaki
kurisaki@fukuoka-u.ac.jp

¹ Department of Chemistry, Faculty of Science, Fukuoka University, 8-19-1 Nanakuma, Jonan-ku, Fukuoka 814-0180, Japan

² Graduate School of Science and Technology, Hirosaki University, 3 Bunkyo-cho, Hirosaki, Aomori 036-8561, Japan

³ Dipartimento di Chimica, Università di Torino, via Pietro Giuria 7, 10125 Turin, Italy

⁴ Present Address: Department of Respiratory Medicine, Graduate School of Medicine Cardiology and Nephrology, Hirosaki University, 5 Zaifu-cho, Hirosaki, Aomori 036-8562, Japan

semiconductor for use in photodetoxification of contaminated water. The sufficient band gap of TiO_2 can generate electron–hole pairs onto the surface of TiO_2 powder. The current hypothesis in photocatalysis is that a surface-adsorbed OH^\cdot radical is the initial product after the hole trapping at the hydrate TiO_2 surface. Hydroxyl radicals have been detected using spin-trapping techniques at room temperature [3, 31–33]. The points of designing effective photocatalysts are that the organic substrate can easily approach the semiconductor surface and be trapped on it, and that the reactive radicals can effectively be generated on the surface. Concentration of an organic pollutant at the semiconductor surface has been achieved by selective doping of the TiO_2 [34, 57], surface modification of the photocatalyst with chelating agents [35], and surface modification of the catalyst with electron acceptor groups [36].

Titanium dioxide (TiO_2) has three crystal phases, anatase, rutile and brookite. Anatase TiO_2 has been extensively investigated owing to its notable functions for photocatalysis and photon-electron transfer [37, 38]. On the other hand, rutile TiO_2 is a thermodynamically stable phase possessing a smaller band gap energy (3.0 eV) than the anatase phase (3.2 eV) [39, 40]. In photocatalysis research, chemists have been paying much greater attention to anatase TiO_2 than to rutile TiO_2 because the anatase form is considered more active than the rutile form. Excellent properties of rutile TiO_2 have been recently disclosed; Beck and Siegel reported the high photocatalytic activity for decomposition of H_2S gas [41], and Ohno et al. [42] reported the high activity of rutile TiO_2 for photooxidation of water with Fe^{3+} as an electron acceptor. The report written by Hurum et al. [43] provides especially valuable information. They explained that the mixed-phase catalysts consisting of anatase TiO_2 and rutile TiO_2 had “hot-spots” at the rutile–anatase interface and these hot spots caused its high photocatalytic activity.

Metal ion-doped TiO_2 , of course, has been studied extensively [44–46] with the purpose of extending the absorption spectrum to visible light. But the results were often controversial; some reports showed that the photooxidativity and photoreducibility were improved through doping, but the other reports showed that the photooxidativity and photoreducibility were reduced. The preparation of lanthanide ion-doped TiO_2 nanoparticles, as well as their photoelectrochemical and photocatalytic properties, have been reported by a few chemists. In previous work, it is reported that the photocatalytic activities increase with modification of TiO_2 with lanthanide ion [47, 48]. In this work, lutetium(III) ion was used to modify materials in order to create high-activity points like hot spots.

Yi et al. and Zhou et al. used electron paramagnetic resonance spectroscopy (EPR) to investigate the formation of Ti^{3+} in the bulk of TiO_2 because the highest concentration of Ti^{3+} corresponds to the strongest absorption intensity of catalyst in the visible-light region [58, 59]. Therefore, EPR measurements for metal ion-doped TiO_2 were really useful for obtaining information about Ti^{3+} in bulk and the effect of doped metal ions.

Here, our experimental results showed that lanthanide ion-doped TiO_2 nanoparticles indicated higher photoreactivity for the photocatalytic degradation of adenosine 5'-triphosphate (ATP) than undoped TiO_2 particles. In addition to these results, the characteristic features of each powder were clearly exhibited by using X-ray diffraction (XRD) measurement, high-performance liquid chromatography

(HPLC) measurement and the Langmuir–Hinshelwood mechanism. In succession, EPR is used as the measurement apparatus to clarify the nature of this powder under both non-irradiation and UV irradiation conditions. At last, this paper proposes the role of lutetium ion doped into TiO_2 structure and the reason for the high photoactivity of Lu- TiO_2 .

Experiment

Materials

Unmodified titanium dioxide (TiO_2) powders denoted by ST-01 ($228.40 \text{ m}^2 \text{ g}^{-1}$ of surface area) as produced by Ishihara Sangyo Kaisha, Ltd., anatase-type TiO_2 and rutile-type TiO_2 as produced by Catalysis Society Japan were used for the reference samples. Titanium(IV) isopropoxide (97.0%; Aldrich Chemical Co. Inc.) and 2-propanol (99.5%; extra pure grade Wako Pure Chemical Industries Ltd.) were used in synthesizing the lutetium ion-doped TiO_2 photocatalysts (Lu- TiO_2). Acetic acid (CH_3COOH , 99.7%, Wako Pure Chemical Industries Ltd.) was used as the pH moderator. Lutetium chloride hexahydrate ($\text{LuCl}_3 \cdot 6\text{H}_2\text{O}$: 99.99+%; Aldrich Chemical Co. Inc.) was also used. ATP disodium salt trihydrate ($\text{C}_{10}\text{H}_{14}\text{N}_5\text{Na}_2 \cdot \text{O}_{13}\text{P}_3 \cdot 3\text{H}_2\text{O}$, 99.0%, Aldrich Chemical Company Inc.) was used as a model compound in photocatalytic studies and also in adsorption experiments with Lu-doped TiO_2 particles.

Synthesis method of metal ion-doped TiO_2 photocatalyst

In order to synthesize the Lu- TiO_2 powder, titanium isopropoxide (10 g , 1.89 mol L^{-1}) was mixed with 2-propanol (10 g , 7.41 mol L^{-1}) in a beaker (inner diameter, 30 mm) and the solution was stirred at room temperature for 30 min . Because the pH value of these solutions was 6, the pH value was adjusted with acetic acid (4 g , 2.91 mol L^{-1} ; 40% for the amount of 2-propanol) to $\text{pH} = 3$, and stirring was continued for another 30 min . Subsequently, the lutetium salt was dissolved in a mixture solution for approximately 2 h . The amount of dissolved salt was 10% of the Ti ion contained in titanium isopropoxide. The solution was then concentrated under reduced pressure (the water bath temperature was $50 \text{ }^\circ\text{C}$ and the pressure was 45 hPa) using a rotary vacuum evaporator. A small amount of white powder was obtained after concentrating the mixture solution. The white Lu- TiO_2 powder was crushed and calcined under aerobic condition using a furnace (Sanstat furnace type SYK-450-T; Sanyo Rigaku Seisakusho K.K.). Before each experiment, powder was dried under vacuum to remove adsorbed water on the powder surface. The calcination temperature was raised to $800 \text{ }^\circ\text{C}$ and the samples were calcined for 9 h . For preparation of non-doped titanium dioxide (denoted as pure TiO_2), the same procedure was used, except for lutetium ion. The sample name and preparation conditions are shown in Table 1. Before EPR measurement, all samples were dried under vacuum to remove adsorbed water on the powder surface.

Table 1 Summary of preparation procedures of the standard, pure TiO₂ and Lu-TiO₂ samples

Sample name	Amount of doped Lu ion (%)	Calcination temperature (°C)	Color of powder
Anatase ^a	–	RT ^c	White
Rutile ^b	–	RT ^c	White
ST-01	–	RT ^c	White
Pure TiO ₂ RT	–	RT ^c	White
Pure TiO ₂ 40	–	400	White
Pure TiO ₂ 50	–	500	White
Pure TiO ₂ 60	–	600	White
Pure TiO ₂ 80	–	800	White
Lu-TiO ₂ RT	10.00	RT ^c	White
Lu-TiO ₂ 40	10.00	400	White
Lu-TiO ₂ 50	10.00	500	White
Lu-TiO ₂ 60	10.00	600	White
Lu-TiO ₂ 80	10.00	800	White

^aAnatase means the anatase-type TiO₂

^bRutile means the rutile-type TiO₂

^cRT means the non-calcined condition

Possible elution of doped metal ions during synthetic or photocatalytic processes was examined repeatedly using EDTA titration, and the results were all negative. Therefore, the doped metal ions were inferred to remain in the catalyst.

Analytical methods

In adsorption experiments, the ATP concentration was determined by means of HPLC apparatus (SHISEIDO NANOSPACE SI-2). HPLC measurement utilized a Capcell Pak C18 AQ column (Shiseido Fine Chemical Co., Ltd, column length 150 mm, internal diameter 1.5 mm, sample size 1.0 μL), which was specially developed for measurement of aqueous samples. The ATP concentrations were evaluated in accordance with the procedures as described in a previous paper [49].

Experimental procedures for photocatalytic reaction

Titanium dioxide and synthesized powder (20 mg) were dispersed into the 0.1 mM ATP solution (20 mL) in a beaker (inner diameter, 35 mm). During the photocatalytic decomposition experiment under UV irradiation (black light, Toshiba; 1.8 mW cm⁻² light intensity at 365-nm wavelength), the suspension sample in the beaker was cooled in an ice bath to prevent hydrolysis of the ATP sample. After the irradiation, the suspension sample was filtered by an Autovial filter (pore size 0.45 μm, AV125UORG, Whatman) and the filtrate was examined with HPLC.

Adsorption of ATP onto the photocatalyst's surface during photocatalytic reaction was examined with the same setups and procedures as used in

photocatalytic decomposition experiment except for UV irradiation. The ATP concentration was periodically evaluated with the HPLC profile. The ATP concentration started to decrease just after TiO_2 and Lu- TiO_2 powders were dispersed into the solution. The decrement was ascribed to adsorption onto the photocatalyst's surface (cf. the text).

Experimental procedures for adsorption reaction: adsorption experiments to obtain the number of adsorption sites (N_S) and the adsorption equilibrium constant (K) of each photocatalytic powder

All ATP concentrations were evaluated with the HPLC profile. The amount of adsorbed ATP was calculated from before and after dispersing each TiO_2 powder into ATP solution. The suspension prepared by mixing each photocatalytic powder (10 mg) with ATP solution (20 mL) in a beaker (inner diameter, 35 mm) was set in an ice bath with an inner temperature of 0.2 °C and was stirred with shielding from light using a magnetic stirrer. The ice bath prevented hydrolysis of ATP. In the experiment of time-dependent behavior of ATP adsorption, an initial ATP concentration was set at 0.1 mM with stirring up to 200 min. On the other hand, the equilibrium concentration of ATP from 0.1 to 0.3 mM was used for estimating N_S and K . The stirring time was kept at 90 min.

XRD measurement and particle size evaluation method

The crystal structures of all sample powders were determined from XRD patterns measured with an X-ray diffractometer (Rigaku, Geigerflex RAD-RA) with a Cu target $K\alpha$ -ray ($\lambda = 1.5405 \text{ \AA}$). Particle size distribution of ST-01 and Lu- TiO_2 60 powder was measured through the courtesy of Sysmex Ltd.

EPR spectroscopy

The X-band (9.5 GHz) EPR spectra of Lu- TiO_2 , pure TiO_2 and ST-01 powders were measured on a spectrometer (EXM; Bruker Analytik) at RT, 77 and 4.4 K. The powder samples, contained in a special quartz tube that can connect to the original vacuum line, were introduced into a resonance cavity. Tube conditions were set to suitable states: aerobic, vacuum, or nitrogen gas conditions. The samples were transferred to a 77-K Dewar flask mounted on the EPR spectrometer, and irradiated by a 468-W cm^{-3} xenon lamp with a 400-nm cutoff filter. In these experiments, samples were irradiated directly in the EPR cavity at 77 K. EPR spectra were recorded before irradiation, at each 3 min during irradiation, after 40 min of irradiation, and at 1 day after irradiation; this set was repeated if necessary.

Results and discussion

Photocatalytic reaction

The ATP solution was irradiated with UV light in the presence of TiO_2 for 90 min. Variation of the HPLC profile with elapsed time is presented in Fig. 1. The signal N means the peak of non-identified products. After 10 min of irradiation, a signal peak for generated adenine was clearly observed at a 9.7-min retention time. As the irradiation time elapsed, the peak due to ATP decreased and that for adenine increased. Since this variation profile of using Lu- TiO_2 60 is similar to that of ST-01, the ATP photodecomposition mechanism also has a good agreement with the previous report [49]. In addition to this, the ATP photodecomposition rate of Lu- TiO_2 60 is faster than that of ST-01. The sample of Lu- TiO_2 60 is considered to have higher photoactivity compared with ST-01.

The adsorption and photocatalytic ability of samples were examined so as to obtain more information regarding the nature of the synthesized samples. The HPLC studies revealed that a considerable amount of the ATP in solution disappeared upon the addition of sample powders, even in the dark. In the absence of sample powders, the ATP concentration remained unchanged within experimental errors. Then, the disappearance of ATP in the dark was concluded to be due to adsorption of ATP onto the surface of TiO_2 (denoted by $\Delta_{\text{ads}}[\text{ATP}]$, hereafter). The $\Delta_{\text{ads}}[\text{ATP}]$ values were repeatedly evaluated under conditions similar to the photocatalytic reactions. The results are summarized in Table 2, where nominal values of disappeared ATP in the photocatalytic reaction $\Delta_{\text{nom}}[\text{ATP}]$ are also listed. The photocatalytic degradation of ATP (denoted by $\Delta_{\text{photo}}[\text{ATP}]$) can be estimated by the difference between $\Delta_{\text{nom}}[\text{ATP}]$ and $\Delta_{\text{ads}}[\text{ATP}]$ values as shown in Table 2. The concentration of photogenerated adenine $\Delta_{\text{photo}}[\text{ADE}]$, as evaluated by HPLC along the elapsed irradiation time, is also summarized in Table 2.

The $\Delta_{\text{photo}}[\text{ADE}]$ values are clearly less than those of the $\Delta_{\text{photo}}[\text{ATP}]$ at the corresponding time in Table 2, except for Lu- TiO_2 . At the end of 90 min of

Fig. 1 Variation of the HPLC profile for ATP degradation during UV irradiation up to 90 min by using Lu- TiO_2 60 sample

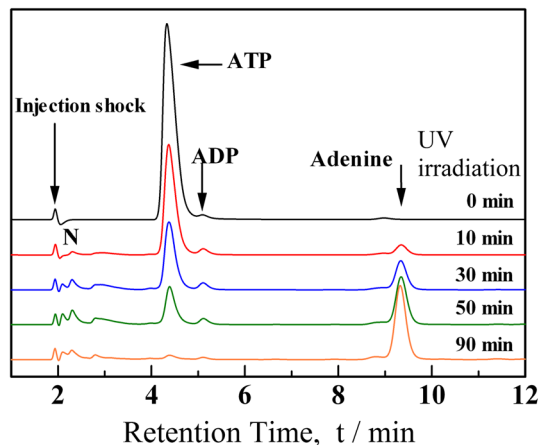


Table 2 Estimated concentrations of the adsorbed and degraded ATP during the UV irradiation

Sample name	$\Delta_{\text{ads}}[\text{ATP}]$ (mM)	$\Delta_{\text{nom}}[\text{ATP}]$ (mM)	$\Delta_{\text{photo}}[\text{ATP}]$ (mM)	$\Delta_{\text{photo}}[\text{ADE}]$ (mM)
Pure TiO ₂ 40	0.001	0.016	0.015	0.005
Pure TiO ₂ 50	0.000	0.020	0.020	0.006
Pure TiO ₂ 60	0.000	0.005	0.005	0.004
Lu-TiO ₂ 40	0.087	0.095	0.009	0.023
Lu-TiO ₂ 50	0.058	0.092	0.034	0.027
Lu-TiO ₂ 60	0.017	0.101	0.084	0.042
ST-01	0.055	0.099	0.044	0.036

Elapsed time is 90 min

Experimental error 0.001 mM

$$\Delta_{\text{photo}}[\text{ATP}] = \Delta_{\text{nom}}[\text{ATP}] - \Delta_{\text{ads}}[\text{ATP}]$$

$\Delta_{\text{photo}}[\text{ATP}]$ means the photogenerated adenine

irradiation, for example, the $\Delta_{\text{photo}}[\text{ADE}]$ value was 78% of the $\Delta_{\text{photo}}[\text{ATP}]$. In other words, the fate of the adenine moiety in the rest of the degraded ATP (ca. 20%) should be still clarified. In the case of Lu-TiO₂ 40, the cause of the large $\Delta_{\text{photo}}[\text{ADE}]$ value as compared to the $\Delta_{\text{photo}}[\text{ATP}]$ value is assumed to create the many ATP molecules adsorbed on the Lu-TiO₂ 40 sample.

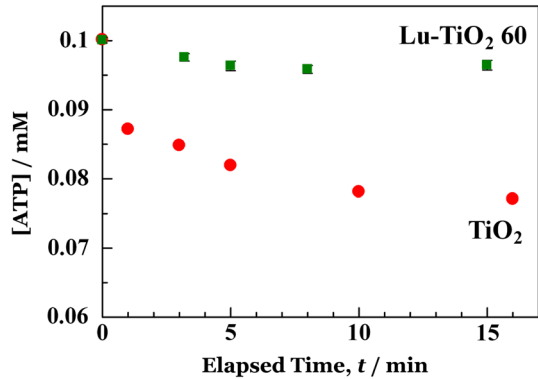
Table 2 indicates that the Lu-TiO₂ 60 sample had higher photodecomposition ability than adsorptive ability; the Lu-TiO₂ 40 had only the highest adsorptive ability. Though all samples of pure TiO₂ had only small photocatalytic ability, Lu-TiO₂ samples may have the adsorptive ability caused by the modification of lutetium ion in basic TiO₂ structure. Then, the difference of adsorptive ability of Lu-TiO₂ was understood to be created from the aggregation of samples by thermodynamic effect during calcination process. For ST-01, this had both photocatalytic and adsorptive ability, but, these were not much higher than the adsorptive ability of Lu-TiO₂ 40 and the photocatalytic ability of Lu-TiO₂ 60.

Adsorption reaction

Greater consideration was given to the details of the adsorptive ability between Lu-TiO₂ 60 and ST-01 was in the subsequent experiments. The ATP solutions with dispersed Lu-TiO₂ and ST-01 powder were prepared and the variation in ATP concentration was followed by HPLC analysis. No signal other than ATP was detected, and the ATP signal intensity simply decreased with elapsed time after dispersing these powders. Then the decrement of ATP signal intensity was ascribed to the amount of ATP adsorption onto the surface of the powders. The ATP concentration in the solution varied along the elapsed time, as shown in Fig. 2.

The ATP concentration in the solution rapidly decreased with the elapsed time at first. The rate of decrease in ATP concentration quickly diminished. As compared with the result of ST-01, that of Lu-TiO₂ 60 was rather different; the ATP concentration in the solution of Lu-TiO₂ 60 approached asymptotic values, as

Fig. 2 Variation of ATP concentration with the elapsed time after dispersing the Lu-TiO₂ 60 powder and standard TiO₂ powder into the ATP solution



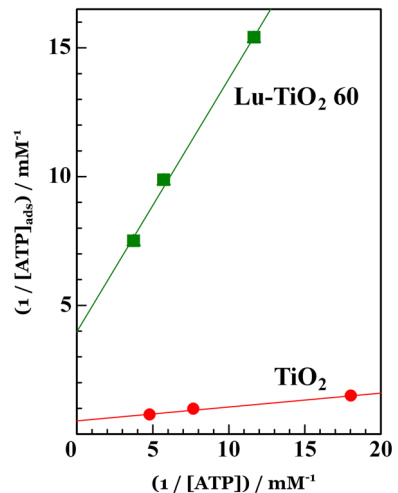
shown in Fig. 2. This result indicated the Lu-TiO₂ 60 powder does not have adsorptive ability like ST-01.

The total number of adsorption sites (N_S) and the adsorption equilibrium constant (K) were estimated by plotting the amount of adsorbed ATP molecules on TiO₂ ($[ATP]_{ads}$) against the ATP concentration in solution ($[ATP]$), or from the Langmuir isotherm for ATP adsorption on TiO₂ powder (Fig. 3):

$$\frac{1}{[ATP]_{ads}} = \frac{1}{N_S} + \frac{1}{KN_S} \frac{1}{[ATP]}$$

The plots give N_S and K for TiO₂ (ST-01) as 1.9 mM and 10 mM⁻¹, and 0.3 mM and 4 mM⁻¹ for Lu-TiO₂ 60, respectively. It is interesting that the properties of these two powders were different from each other: N_S and K for ST-01 were about 6.3 times and 2.5 times rather than those of Lu-TiO₂, respectively.

Fig. 3 Estimation of N_S and K values by plotting the amount of adsorbed ATP on TiO₂ against the ATP concentration in solution



XRD measurement

Figure 4 shows the XRD patterns of the standard powder (anatase, rutile and ST-01) and synthesized powders. The signal of ST-01 is rather broader than the other standard samples because this powder comprised $> 90\%$ anatase and $< 10\%$ rutile TiO_2 particles, and the size of ST-01 powder is rather smaller than the other standard samples (see Fig. 4a). Almost all profiles of pure TiO_2 samples may be ascribed to an anatase or rutile signal. One can confirm that the A signal (anatase TiO_2) gradually increases with the increment of calcined temperature and that the temperature of phase transformation from anatase to rutile is 600°C . Signals, both anatase and rutile, calcined at high temperature, $> 600^\circ\text{C}$, are sharper than that of anatase and rutile calcined at low temperature $< 500^\circ\text{C}$. These changes suggest that the particle size increases because these particles are aggregated by a thermodynamic effect. On the other hand, the profile of Lu-TiO_2 shows the temperature of phase transformation is 800°C and the particle sizes of these samples are rather smaller than that of the pure TiO_2 samples. These results are caused for doping the lutetium ion into TiO_2 structure using the present method. One may guess that this sample would have the interface between anatase and rutile particles created by the doped lutetium ion having a large ionic radius as compared to a titanium ion or oxygen ion.

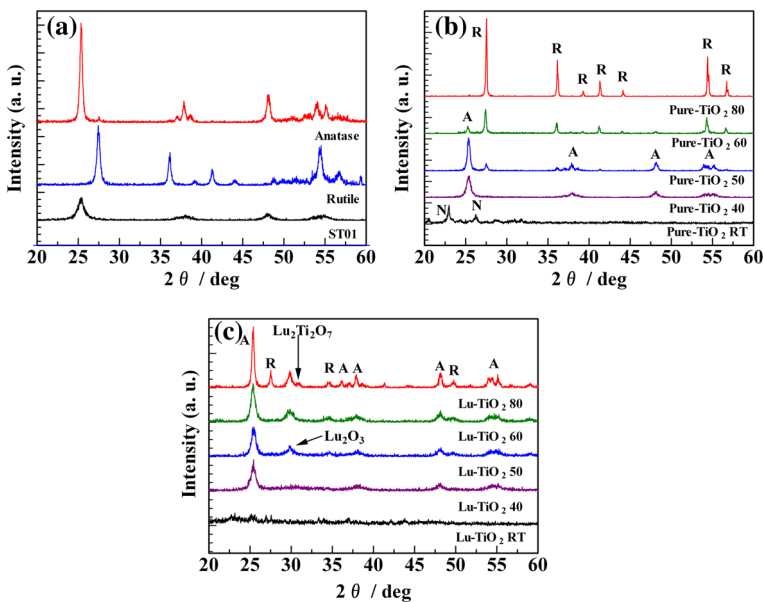


Fig. 4 XRD profiles of the **a** standard, **b** pure TiO_2 and **c** Lu-TiO_2 samples. The A and R marks in (b) mean an anatase and rutile signal ascribed from the profile in (a), respectively, and N means a non-identified signal

EPR spectroscopy

EPR spectra of Lu-TiO₂ 60 (Fig. 5) were recorded at RT (A), 77 K (B) and 4.4 K (C) to investigate the spectral feature. Spectra of pure TiO₂ and ST-01 as a reference are indicated in Figs. 6 and 7, respectively. For all three samples, comparison of spectra at RT (A) and 77 K (B) shows that the spectra obtained at 77 K (B) is better in signal-to-noise ratio than those in RT (A). Furthermore, the spectrum at 4.4 K indicates well-resolved signals compared to that in 77 K. It means that a temperature lower than 77 K could make the rate of spin–lattice relaxation slower. However, the experimental condition of 4.4 K was not suitable for UV irradiation, so that 77 K was chosen to measure EPR spectra in this study. Forms of two spectra in Figs. 5b and 6b were mutually resemblance, and differed from the spectrum in Fig. 7b. The difference in the spectral feature may occur from the powder structure. There can be two reasons; the ratio of anatase-to-rutile and the synthesis method.

Figure 8 depicts the variation of EPR spectra for Lu-TiO₂ 60 during UV irradiation up to 40 min: panel (A) shows the spectra attributable to each UV irradiation time, panel (B) superimposed the spectra on a pre-irradiation spectrum and panel (C) portrays the spectra obtained before and after UV irradiation. An identical experiment (called as the second experiment) was repeated using the same powder and experimental conditions after the primary experiment (Fig. 8). The signals indicated by a-c in Fig. 8 are discussed here. Panels (A) and (B) show that peak a and peak c were created after UV irradiation and that peak c decreased gradually during 40 min. On the other hand, panel (C) shows clearly that peaks a

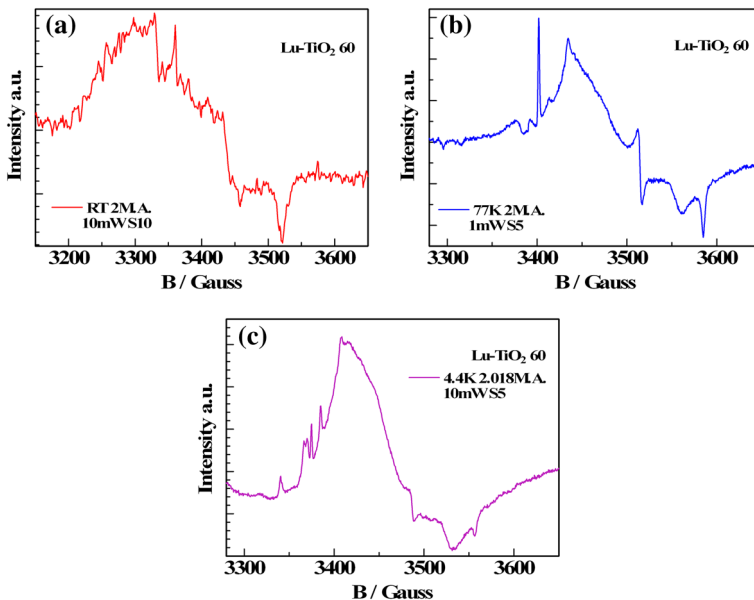


Fig. 5 X-band EPR spectra of Lu-TiO₂ recorded at **a** RT, **b** 77 K and **c** 4.4 K. Measurement conditions are indicated in each figure

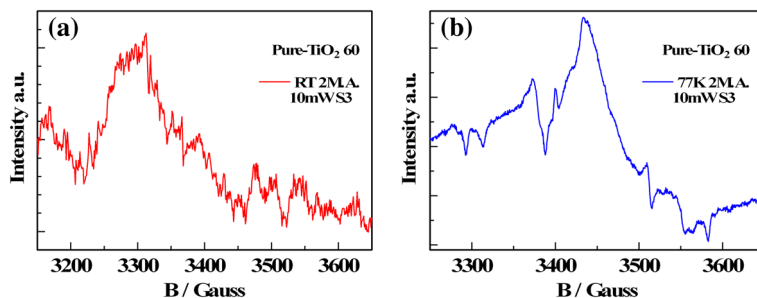


Fig. 6 X-band EPR spectra of pure TiO_2 recorded at **a** RT and **b** 77 K. Measurement conditions are indicated in each figure

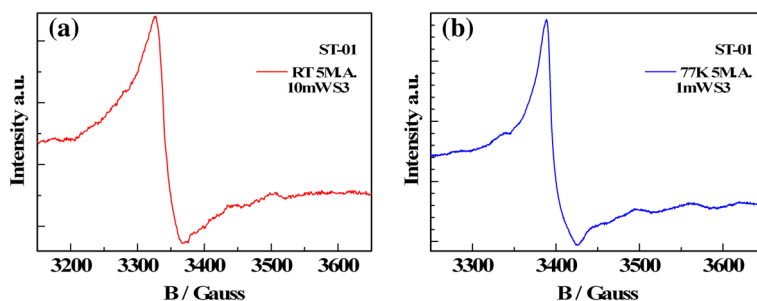


Fig. 7 X-band EPR spectra of ST-01 recorded at **a** RT and **b** 77 K. Measurement conditions are indicated in each figure

and c disappeared 1 day after UV irradiation. The intensity of all peaks in the second experiment became smaller than those obtained in the first experiment. The variation of EPR spectra at 3 min was greatest in comparison with other spectra. These results mean that the generation of those peaks, a and c, were moderately related to the electron–hole pair generated upon adsorption of UV light energy by Lu- TiO_2 60, and reaction needed UV irradiation at least for 3 min.

Similar experiments were carried out with pure TiO_2 60 and ST-01 (Figs. 9, 10) as reference experiments. The signals indicated by d–i in Figs. 9 and 10 are discussed here. The intensity of peak d just after UV irradiation (denoted by 0 min) becomes the biggest peak compared with that given at another irradiation time. On the other hand, the peak f did not hold its intensity and formed under UV irradiation up to 30 min, and then the peak e generated with UV irradiation could be observed present for a period up to 30 min. As the positions of peaks d (3372.9 Gauss) and f (3401.4 Gauss) agreed well with those of the corresponding peaks a (3372.9 Gauss) and b (3401.4 Gauss) in Fig. 8, these peaks are considered to have the same origin. In case of ST-01 in Fig. 10, variations of EPR spectra differ from those of the other two samples. It is readily noticed that the three peaks (indicated by g, h and i) are observed only during UV irradiation and that the forms of the spectra before and after UV irradiation remained the same. Three minutes of UV irradiation needed for the ST-01 showed the biggest change. Peaks g–i (3379.5, 3401.8 and 3413.9 Gauss,

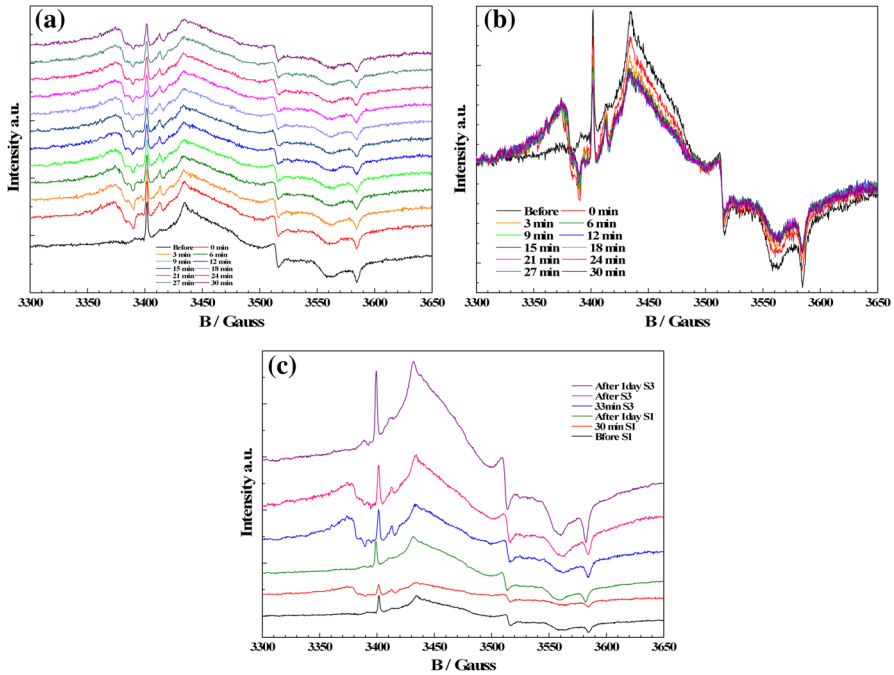


Fig. 8 Variation of EPR spectra for Lu-TiO₂ 60 during UV irradiation up to 40 min. **a** Spectra due to each UV irradiation time, **b** superimposed spectra on a before spectrum and **c** spectra of before and after UV irradiation

respectively), however, are regarded as having the same origin as the signals ($a \approx d \approx 3372.0$, $b \approx h \approx 3401.0$ and $c = 3412.8$ Gauss, respectively) in Figs. 8a and 9a.

In order to confirm the condition of powders, interesting experiments were carried out using the same apparatus. After two cycles of UV irradiation experiments, the sample powder was calcined in a nitrogen gas condition, and EPR spectrum was obtained at RT (Fig. 11). Then the sample was calcined in an oxygen gas condition, and EPR was measured. Sharp signals (j and k) in Fig. 11 appeared at around 3350 Gauss. In the 'before' condition, the signals j and k are relatively broad. Both the signal intensity increase in signal j when the temperature increases from 200 °C at 30 min to 200 °C at 2 h; this signal disappears at the calcination temperature of 300 °C. In addition, signal k disappears at 200 °C by 30 min. Upon re-oxidation at 300 °C by 2 h, signal j appears weakly at the same position, but signal k does not appear at all. These results explain that the calcination treatment using nitrogen gas reveals various Ti³⁺ sites that are produced in the labile TiO₂ structure on Lu-TiO₂ 60 surface. Consequently, re-oxidation by oxygen gas converts Ti³⁺ ions on the surface of Lu-TiO₂ 60 to Ti⁴⁺. The same experiments were carried out for pure TiO₂; the signal j disappeared by oxidation treatment at 200 °C. It is notable that the temperature of this treatment was lower

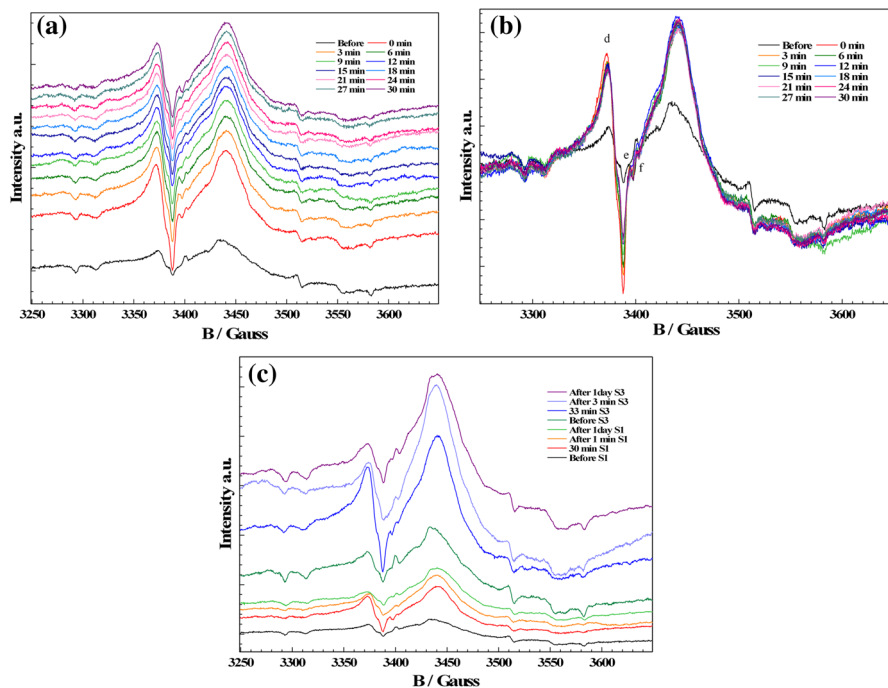


Fig. 9 Variation of EPR spectra for pure TiO_2 60 during UV irradiation up to 40 min. **a** Spectra due to each UV irradiation time, **b** superimposed spectra on a before spectrum and **c** spectra of before and after UV irradiation. (Color figure online)

than that of Lu-TiO_2 60. It shows that the lutetium ion modified the TiO_2 structure and made a more labile Ti^{3+} spot on the surface structure.

Many chemists have already reported EPR spectra for various TiO_2 , not only for powder, but also for the colloidal state [43, 50–56]. No literature has confirmed the presence of peaks A, B, D and E in Fig. 12(a). These peaks are considered characteristic of the method of sample synthesis because the ST-01 had no peaks like A, B, D and E (see Figs. 7, 10). Howe explained that some peaks appearing in the region of 3350–3600 Gauss were ascribed to Ti^{3+} present in the TiO_2 structure and O^- created by trapped holes [50–52]. Signals ascribed to anatase TiO_2 and rutile TiO_2 are therefore easily found in the region of 3350–3600 Gauss. The respective g -values of anatase and rutile are $g_{//} = 1.957$, $g_{\perp} = 1.990$ and $g_{//} = 1.940$, $g_{\perp} = 1.975$. Figure 12 and Table 3 show EPR spectra just after UV irradiation for 10 s (0 min means UV irradiation for 10 s) and g -values calculated from each spectrum in Fig. 12. One may understand that two powders, Lu-TiO_2 60 and pure TiO_2 60, have g -values attributed to Ti^{3+} ions in the anatase and rutile structures; subscripts of K, C and L may look just like anatase g_{\perp} and rutile $g_{//}$ and g_{\perp} . The $g_{//}$ values of anatase TiO_2 were not obtained because they were obscured by a broad rutile signal. From these spectra, the main structure of two powders was considered to be as follows: the Lu-TiO_2 60 has a lot of anatase structure and the pure TiO_2 60

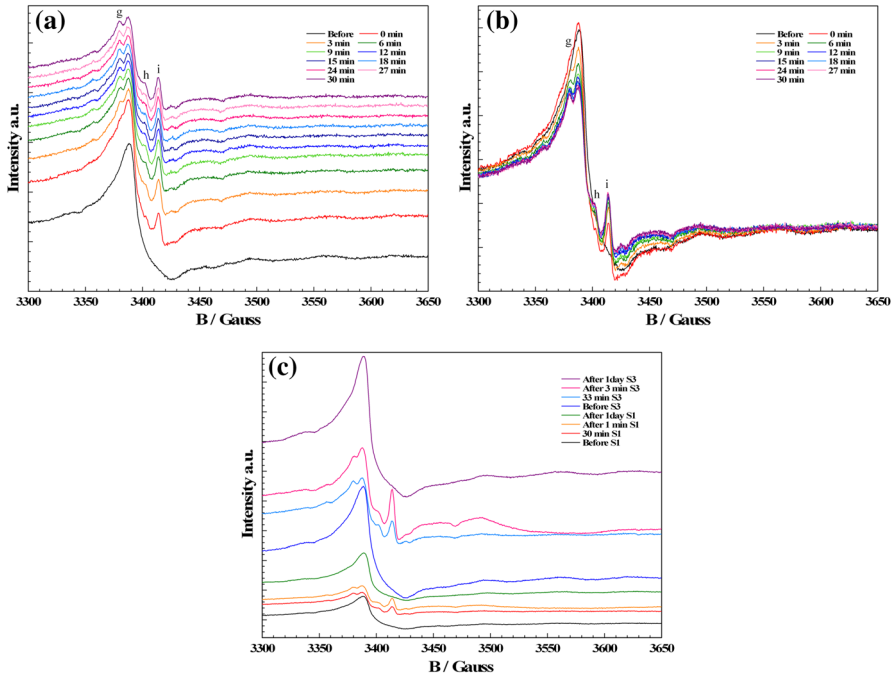


Fig. 10 Variation of EPR spectra for ST-01 during UV irradiation up to 40 min. **a** Spectra due to each UV irradiation time, **b** superimposed spectra on a before spectrum and **c** spectra of before and after UV irradiation. (Color figure online)

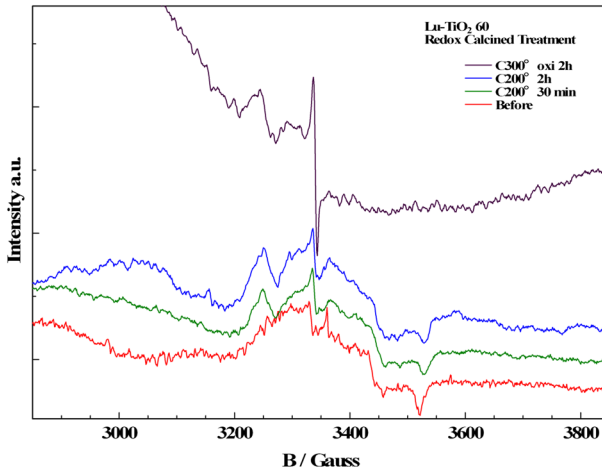


Fig. 11 Redox calcined EPR spectra of Lu-TiO₂ 60 recorded at 77 K. Measurement conditions are indicated in each figure. (Color figure online)

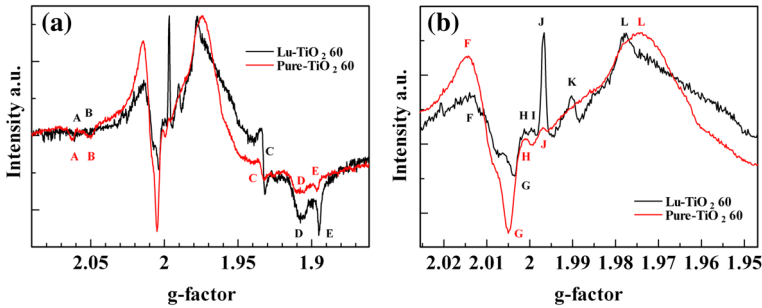


Fig. 12 EPR spectra for Lu-TiO₂ 60 and pure TiO₂ 60 under UV irradiation at different regions of *g*-values of: **a** 2.090–1.861 and **b** 2.026–1.947. (Color figure online)

Table 3 The *g*-values obtained from EPR spectra of Lu-TiO₂ 60 and pure TiO₂ 60 in Fig. 12

Signal index	<i>g</i> -Value Lu-TiO ₂ 60	Signal index	<i>g</i> -Value pure TiO ₂ 60
A	2.061	A	2.062
B	2.052	B	2.049
C	1.933	C	1.933
D	1.907	D	1.907
E	1.895	E	1.895
F	2.013	F	2.014
G	2.003	G	2.004
H	2.001	H	2.000
I	1.999	–	–
J	1.997	J	1.996
K	1.990	–	–
L	1.978	L	1.973

has many rutile structures and a small amount of anatase structure. The XRD results of Fig. 4b, c were in good agreement with these EPR results.

Howe et al. [50] experimented with hydrated and deuterated anatase and their works proposed that *g*-tensor values for the low-field signal ($g_1 = 2.016$, $g_2 = 2.012$ and $g_3 = 2.002$) arose from trapped positive holes at lattice oxide ions (O⁻ radical anion). They explained that the theoretical expressions for the *g*-tensor components of O⁻ are in first order:

$$g_{zz} = g_e$$

$$g_{xx} = g_e + \frac{2\lambda}{E_x}$$

$$g_{yy} = g_e + \frac{2\lambda}{E_y}$$

where λ is the spin–orbit coupling constant for oxygen (0.014 eV) and E_x and E_y are the energy separation for the orbital containing the unpaired electron (p_z) from the p_x and p_y orbitals, respectively. In addition to this, the g -tensor components for the low-field signal could be fitted to these expressions, yielding $E_x = 2.00$ eV and $E_y = 2.80$ eV, respectively. Though the low-field signal also formed on irradiation in vacuo is more difficult to identify and the sample conditions are remarkably different, the behavior under UV irradiation treatment and g -tensor values of signals F and G is thought to be similar to that of the low-field signal that appeared in Howe's works. From the g -values, $E_{\perp} = 2.5$ eV for Lu-TiO₂ 60 and $E_{\perp} = 2.3$ eV for pure TiO₂ 60. It is, therefore, possible to conclude that F and G are ascribed to the signal of an O⁻ radical anion.

Conclusions

The most effective photocatalytic powder for ATP decomposition in the present study was unquestionably the Lu-TiO₂ 60 sample. This highest photoactivity could be achieved by doping the lutetium ion into basic TiO₂ structure and by calcination under aerobic condition at 600 °C. This powder features a low adsorptive ability of ATP during the photodecomposition reaction. Then, the observed decrement in ATP concentration should be ascribed to the reaction of photogenerated radicals at the surface of Lu-TiO₂ 60. As this powder consisted of anatase and rutile TiO₂ fine particles, the high photoactivity was ascribed to the interaction between anatase and rutile TiO₂ fine particle with doped lutetium ion. In addition, the presence of Lu₂Ti₂O₇ and Lu₂O₃ particles might be partly responsible for the high photocatalytic property of Lu-TiO₂ 60.

Howe et al. proposed a possible pathway for the formation of O⁻: (1) the primary photochemical event is a creation of holes and electrons, (2) electrons are trapped at Ti⁴⁺ sites to form Ti³⁺ and holes at subsurface oxide ions to form O⁻. Therefore, the EPR signals F and G in Fig. 12 are considered to be the generated O⁻ under UV irradiation. The property of the peaks C, K and L agree with that of the Ti³⁺ in anatase and rutile structure; the signals of these paramagnetic species were decreasing under UV irradiation. At the point of intensity decrement, here, the signals H, I and J are also ascribed to the generated Ti³⁺ under UV irradiation. Especially, peak J suggests that another type of structure consisting of Ti³⁺ or O⁻ may exist in the two powders, Lu-TiO₂ 60 and pure TiO₂ 60, and the preferred new structure is Lu-TiO₂ 60 rather than pure TiO₂ 60. Results of redox calcination treatment indicate the labile Ti³⁺ spot in the surface structure of Lu-TiO₂ 60.

This work found that the high photocatalytic ability of Lu-TiO₂ 60 results from the presence of labile Ti³⁺ spots in the Lu-TiO₂ 60 surface structure created from the Lu³⁺ ions doped into TiO₂ structure using the original method. In other words, the role of the Lu³⁺ ion is to create the different type of Ti³⁺ spots on the powder's surface, and the recombination of electron–hole pairs required a longer time compared with pure TiO₂ 60 and ST-01 powders.

Acknowledgements Support for the X-band EPR spectrometer and analytical studies was provided by staff of the Dipartimento di Chimica in Università di Torino. The authors wish to thank Prof. Masakazu Anpo in Osaka Prefecture University for his kindly technical supports. Thanks also go to Prof. Hirofumi Tomita in the Graduate School of Medicine Cardiology and Nephrology, Hirosaki University, who always give us understanding for this study.

References

1. S.N. Frank, A.J. Bard, *J. Phys. Chem.* **81**, 1484 (1977)
2. B. Kraeutler, A.J. Bard, *J. Am. Chem. Soc.* **100**, 4317 (1978)
3. C.D. Jaeger, A.J. Bard, *J. Phys. Chem.* **83**, 3146 (1979)
4. A.R. Gonzalez-Elipe, G. Munuera, J. Soria, *J. Chem. Soc. Faraday Trans. 1*(75), 748 (1979)
5. M. Fujihira, Y. Satoh, T. Osa, *Nature (London, U. K.)* **293**, 206 (1981)
6. I. Izumi, F.-R.F. Fan, A.J. Bard, *J. Phys. Chem.* **85**, 218 (1981)
7. M.A. Fox, C.-C. Chen, *J. Am. Chem. Soc.* **103**, 6757 (1981)
8. S. Teratani, J. Nakamichi, K. Taya, K. Tanaka, *Bull. Chem. Soc. Jpn.* **55**, 1688 (1982)
9. E. Borgarello, J. Desilvestro, M. Grätzel, E. Pelizzetti, *Helv. Chim. Acta* **66**, 1827 (1983)
10. M. Barbeni, E. Pramauro, E. Pelizzetti, *Nouv. J. Chim.* **8**, 292 (1984)
11. D. Bahnemann, A. Henglein, J. Lilie, L. Spanhel, *J. Phys. Chem.* **88**, 709 (1984)
12. M. Barbeni, E. Pramauro, E. Pelizzetti, E. Brogarello, M. Grätzel, N. Serpone, *Nouv. J. Chim.* **8**, 547 (1984)
13. A.P. Hong, D.W. Bahnemann, M.R. Hoffmann, *J. Phys. Chem.* **91**, 2109 (1987)
14. G.T. Brown, J.R. Darwent, *J. Phys. Chem.* **88**, 4955 (1984)
15. H. Hidaka, H. Kubota, M. Grätzel, E. Pelizzetti, N. Serpone, *Nouv. J. Chim.* **9**, 67 (1985)
16. K. Okamoto, Y. Yamamoto, H. Tanaka, A. Itaya, *Bull. Chem. Soc. Jpn.* **58**, 2023 (1985)
17. E. Pelizzetti, M. Barbeni, E. Pramauro, N. Serpone, E. Borgarello, M. Jamieson, H. Hidaka, *Chim. Ind. (Milan, Italy)* **67**, 623 (1985)
18. M. Anpo, T. Shima, Y. Kubokawa, *Chem. Lett.* **14**, 1799 (1985)
19. M. Barbeni, E. Pramauro, E. Pelizzetti, E. Borgarello, N. Serpone, M.A. Jamieson, *Chemosphere* **15**, 1913 (1986)
20. R.W. Matthews, *Water Res.* **20**, 569 (1986)
21. N. Serpone, E. Borgarello, R. Harris, P. Cahill, M. Borgarello, E. Pelizzetti, *Sol. Energy Mater.* **14**, 121 (1986)
22. R. Matthews, *Aust. J. Chem.* **40**, 667 (1987)
23. S. Tunesi, M.A. Anderson, *Chemosphere* **16**, 1447 (1987)
24. A. Heller, Y. Degani, D.W. Johnson Jr., P.K. Gallagher, *J. Phys. Chem.* **91**, 5987 (1987)
25. R.W. Matthews, *J. Phys. Chem.* **91**, 3328 (1987)
26. H. Al-Ekabi, N. Serpone, *J. Phys. Chem.* **92**, 5726 (1988)
27. J. Cunningham, S. Srijaranai, *J. Photochem. Photobiol. A* **43**, 329 (1988)
28. C.S. Turchi, D.F. Ollis, *J. Phys. Chem.* **92**, 6852 (1988)
29. A. Henglein, *Top. Curr. Chem.* **92**, 5726 (1988)
30. C. Kormann, D.W. Bahnemann, M.R. Hoffmann, *Environ. Sci. Technol.* **22**, 798 (1988)
31. J.R. Harbour, M.L. Hair, *J. Phys. Chem.* **83**, 652 (1979)
32. E.M. Ceresa, L. Burlamacchi, M. Visca, *J. Mater. Sci.* **18**, 289 (1983)
33. V. Brezova, A. Stasko, L. Lapcik Jr., *J. Photochem. Photobiol. A* **59**, 115 (1991)
34. K.T. Ranjit, H. Cohen, I. Willner, S. Bossmann, A.M. Braun, *J. Mater. Sci.* **34**, 5273 (1999)
35. Y. Mao, C. Schöneich, K.-D. Asmus, *J. Phys. Chem.* **95**, 10080 (1991)
36. K.T. Ranjit, E. Joselevich, I. Willner, *J. Photochem. Photobiol. A* **99**, 185 (1996)
37. M.A. Fox, M.T. Dulay, *Chem. Rev.* **93**, 341 (1993)
38. T. Moritz, J. Reiss, K. Diesner, D. Su, A. Chemseddine, *J. Phys. Chem. B* **101**, 8052 (1997)
39. A. Sclafani, J.M. Herrman, *J. Phys. Chem.* **100**, 13655 (1996)
40. C. Kormann, D.W. Bahnemann, M.R. Hoffmann, *J. Phys. Chem.* **92**, 5196 (1988)
41. D.D. Beck, R.W. Siegel, *J. Mater. Res.* **7**, 2840 (1992)
42. T. Ohno, D. Haga, K. Fujihira, K. Kaizaki, M. Matsumura, *J. Phys. Chem. B* **101**, 6415 (1997)
43. D.C. Hurum, A.G. Agrios, K.A. Gray, T. Rajh, M.C. Thurnauer, *J. Phys. Chem. B* **107**, 4545 (2003)
44. J. Soria, J.C. Conesa, V. Auguliano et al., *J. Phys. Chem.* **95**, 274 (1991)

45. Z. Luo, Q.H. Gao, J. Photochem. Photobiol. A Chem. **63**, 367 (1992)
46. W. Choi, A. Thermin, M.R. Hoffmann, J. Phys. Chem. **98**, 13669 (1994)
47. N. Sakaguchi, S. Matsuo, T. Kurisaki, T. Matsuo, H. Wakita, Res. Chem. Intermed. **32**, 95 (2006)
48. N. Sakaguchi, K. Yamada, S. Matsuo, T. Matsuo, H. Wakita, Res. Chem. Intermed. **32**, 171 (2006)
49. N. Sakaguchi, S. Matsuo, K. Yamada, T. Matsuo, H. Wakita, Res. Chem. Intermed. **30**, 879 (2004)
50. R.F. Howe, M. Grätzel, J. Phys. Chem. **91**, 3906 (1987)
51. R.F. Howe, M. Grätzel, J. Phys. Chem. **89**, 4495 (1985)
52. O.I. Micic, Y. Zhang, K.R. Cromack, A.D. Trifunac, M.C. Thurnauer, J. Phys. Chem. **97**, 7277 (1993)
53. Y. Nakaoka, Y. Nosaka, J. Photochem. Photobiol. A **110**, 299 (1997)
54. K. Ishibashi, Y. Nosaka, K. Hashimoto, A. Fujishima, J. Phys. Chem. B **102**, 2117 (1998)
55. T. Hirakawa, Y. Nakaoka, J. Nishino, Y. Nosaka, J. Phys. Chem. B **103**, 4399 (1999)
56. T. Hirakawa, H. Kominami, B. Ohtani, Y. Nosaka, J. Phys. Chem. B **105**, 6993 (2001)
57. Y. Cong, B. Tian, J. Zhang, Appl. Catal. B **101**, 376 (2011)
58. Q. Yi, Y. Zhou, M. Xing, J. Zhang, Res. Chem. Intermed. **42**, 4181 (2016)
59. Y. Zhou, Y. Liu, P. Liu, W. Zhang, M. Xing, J. Zhang, Appl. Catal. B **170–171**, 66 (2015)